ELSEVIER

Journal of Molecular Catalysis A: Chemical 100 (1995) 115–127

JOURNAL OF MOLECULAR CATALYSIS A: CHEMICAL

Sn-promoting mechanism for ketone hydrogenation over Rh/SiO_2

Ken-ichi Yoshikawa, Yasuhiro Iwasawa *

Department of Chemistry, Graduate School of Science, The University of Tokyo, Hongo, Bunkyo-ku, Tokyo 113, Japan

Received 1 June 1995

Abstract

Hydrogenation of acetophenone, 2-butanone, styrene and 1-hexene over $Rh–Sn/SiO_2$ in heterogeneous liquid phase reaction systems was studied by in situ EXAFS, FT-IR, TEM, analytical TEM, CO and H_2 adsorption measurements. The catalytic activity of Rh/SiO_2 for hydrogenation of acetophenone and 2-butanone increased by a factor of 5–500 by Sn addition, showing a maximum activity at surface composition $Sn_s/Rh_s = 1.5$, whereas hydrogenation of styrene and 1-hexene decreased monotonously and drastically by Sn addition. In situ Sn K-edge EXAFS of the well characterized CVD-$Rh–Sn/SiO_2$ catalyst prepared by using $Sn(CH_3)_4$ vapor suggested that oxygen of C=O group makes a bond with Sn atom upon acetophenone adsorption.

Keywords: EXAFS; Hydrogenation; Ketone; $Rh–Sn/SiO_2$

1. Introduction

Supported-metal catalysis is often drastically improved by small amounts of second metal additives, showing not only increase in activity but also change in selectivity [1,2]. We treat with Sn-promoting effects on reactant preference and activity enhancement on Rh/SiO_2, and with promoting mechanism from structural points of view at the bimetallic surfaces in the hydrogenation reactions of C=O and C=C double bonds.

Sn metal has no significant catalytic activity by itself for most reactions because it hardly interacts with H_2, hydrocarbons, CO, NO and so on, while Sn has been used as a promoter for supported transition metal catalysts to enhance their catalytic performance or to decrease deactivation rate, due to isolation and/or electronic modification of the surface transition metal atoms. Promoter effects due to the dilution of the metal sites active for undesirable carbonaceous material deposition and due to the weakening of the adsorption bond by electronic modification in $Pd–Sn/SiO_2$ and $Ni–Sn/SiO_2$ systems are caused by the formation of alloys or intermetallic compounds [3,4].

In addition, there is the third additive effect owing to direct interaction of Sn with the oxygen atom of a reactant because Sn has greater affinity with oxygen than most of transition metals [5,6]. Tomishige et al. designed and characterized the bimetallic surface of $Rh–Sn/SiO_2$ catalysts, which were prepared by using a selective reaction between Rh particles supported on SiO_2 and $Sn(CH_3)_4$ vapor [7–10]. The obtained $Rh–Sn/SiO_2$ catalysts showed much higher activity than Rh/SiO_2 and coimpregnation $Rh–Sn/SiO_2$ catalysts for the NO dissociation and the catalytic NO reduction by H_2. In the selective hydrogenolysis of ethyl acetate into ethanol over $Rh–Sn/SiO_2$, $Ru–Sn/SiO_2$, and $Ni–Sn/SiO_2$ catalysts which

* Corresponding author.

1381-1169/95/$09.50 © 1995 Elsevier Science B.V. All rights reserved
SSDI 1381-1169(95)00135-2

were prepared by the reaction between $Sn(C_4H_9)_4$ and oxidized Rh/SiO_2, Ru/SiO_2, and Ni/SiO_2, respectively, the selectivity to ethanol was much higher than the corresponding monometallic Rh/SiO_2, Ru/SiO_2, or Ni/SiO_2. It has also been suggested that Sn atom interacts with the oxygen atom of the carbonyl group of ethyl acetate [11–14].

Hydrogenation of unsaturated C=O compounds has been a target reaction to explore the promotion mechanism of Sn, but it remains not clear whether interaction of Sn with C=O oxygen atom is present. It has been reported that addition of Sn or Ge to Pt/Nylon catalyst and addition of Sn to Ru/C catalyst increased the activity and selectivity to the unsaturated alcohols in hydrogenation of α,β-unsaturated aldehydes [15–17]. It was suggested that acidic properties of Sn ions activate the carbonyl group to increase a positive charge on the C=O carbon atom and that formation of the Pt–Sn solid solution increases the electron density of platinum sites to generate more negative chemisorbed hydrogen.

It was also reported from experiments by fixed-bed flow reactor that addition of Sn to Pt/SiO_2 catalysts increased the activity and the selectivity to unsaturated alcohols in hydrogenation of α,β-unsaturated aldehydes [18–21]. Three effects were proposed as to this result. First, Sn makes Pt ensembles smaller and inhibits multiple adsorption of the reactant, and depresses hydrogenation of C=C and hydrogenolysis. Second, the activity of $Pt–Sn/SiO_2$ is higher than that of Pt/SiO_2 due to less carbonaceous or polymeric deposits. Third, Sn interacts with dissociatively adsorbed species of aldehydes and activated hydrogenation of C=O. But the latter two effects were suggested to be negligible in ketone hydrogenations. And from the presence of the induction period and the influence on the selectivity caused by varying the pretreatment conditions, Marinelli et al. suggested that Sn^{n+} ions were present in their catalysts even after the catalyst reduction [18,19].

Basset et al. reported that in the hydrogenation of citral over Rh–Sn-alloy/SiO_2, citronellol was obtained at high selectivity, while citronellal was preferentially obtained over Rh/SiO_2 [22–25]. Moreover, they reported that geraniol and nerol were obtained at high selectivity over the Rh–Sn/SiO_2 catalyst in which Sn was present in the form of the superficial organobimetallic complex on the Rh particles.

The aim of this study is (1) to examine the catalytic activity of Rh–Sn/SiO_2 catalysts prepared in two different ways for ketone and alkene hydrogenation reactions as a function of Sn content, (2) to compare the Sn content-dependent catalytic performance for C=O hydrogenation and C=C hydrogenation, (3) to characterize the surface bimetallic reaction sites by EXAFS, TEM, analytical TEM, FT-IR, and adsorption measurements, and (4) to observe direct interaction between Sn atom and carbonyl group of ketones by EXAFS.

2. Experimental

2.1. Catalyst preparation

Catalysts used in this study were prepared by two different methods. One is on impregnation method and the catalysts prepared by this method are denoted as Imp-Rh–Sn/SiO_2. The other is a chemical vapor deposition method by using tetramethyl tin. The catalysts prepared by this method are denoted as CVD-Rh–Sn/SiO_2. Tin atoms in CVD-Rh–Sn/SiO_2 have been demonstrated to be located at the surface of bimetallic particles [5,9].

Imp-Rh–Sn/SiO_2 catalysts were prepared by the following procedure. SiO_2 (Aerosil O×50: 50 $m^2\ g^{-1}$) was impregnated with an aqueous solution of $Rh(NO_3)_3$, followed by evaporating the solvent with continuous stirring. After that, the resultant samples were dried at 393 K for 12 h, followed by calcination in air at 623 K for 2 h. The Rh loading was controlled to be 3.0 wt%. The obtained Rh/SiO_2 samples were impregnated with a methanol solution of a given amount of $SnCl_2$, followed by evaporating the solvent with continuous stirring. The resultant samples were dried at 393 K for 12 h, followed by calcination in air at 623 K for 2 h. The impregnation catalysts

were reduced with hydrogen (40 kPa) at 673 K for 1 h and evacuated for 0.5 h at 673 K in situ before each run.

CVD-Rh–Sn/SiO_2 catalysts were prepared according to the procedure reported by Tomishige et al [5]. The procedure is briefly summarized as follows. SiO_2 (Aerosil 200: 200 m^2 g^{-1}) was impregnated with a methanol solution of $RhCl_3 \cdot 3H_2O$ (Soekawa Chemical Co.), followed by dry at 373 K for 12 h and by reduction with H_2 at 573 K for 1 h. The obtained Rh particles on SiO_2 were reacted with given amounts of $Sn(CH_3)_4$ (Soekawa Chemical Co.) vapor at 423 K for 15 min in a closed circulating system (dead volume: 200 ml). It has been demonstrated that $Sn(CH_3)_4$ vapor completely reacted with Rh-particle surfaces selectively, not with SiO_2 surfaces, under this condition. The samples were finally reduced with H_2 at 573 K for 1 h, followed by evacuation in situ before use as catalysts and also before each run. The loading of Rh was controlled to be 1.0 wt%, while the Sn/Rh atomic ratio was varied in the range 0–1.0.

The notation 'Sn/Rh' means the ratio of the total number of Sn atoms to that of Rh atoms, while the notation 'Sn_s/Rh_s' means the ratio of the number of the surface Sn atoms to that of the surface Rh atoms.

2.2. Reactant purifications

Acetophenone and styrene were distilled in an Ar flow and stored in Schlenk bottles. 2-Butanone, 1-hexene, and hexane of research grade were commercially obtained and were used without further purification.

2.3. Catalytic reactions

A typical procedure is as follows. Hydrogenation reactions were carried out in a 50-ml Schlenk bottle-type reactor, which was connected to a high-vacuum line and to an Ar flow line through a reflux condenser. 0.2 g of the catalyst was pretreated as above mentioned in the Schlenk bottle-type reactor, and then 20 ml of a reactant was introduced into the reactor under Ar flow. A catalytic reaction was carried out at 323 K under atmospheric pressure of H_2 (a constant pressure) with continuous stirring at a rate of 1200 rpm. The catalytic reaction was followed by analyzing a 2 μl sample of the reaction mixture at intervals by a gas chromatograph using a 4-m column of PEG-HT for hydrogenation of acetophenone or styrene, and a 4-m column of PEG-1500 for hydrogenation of 2-butanone or 1-hexene.

2.4. H_2 and CO adsorption

The amounts of H_2 and CO adsorbed on the catalysts were volumetrically measured in a closed circulating system (dead volume: 80 ml) under H_2 or CO of 20 kPa at 273 K. The amount of irreversible adsorption was estimated by subtracting the amount of reversible adsorption at the second adsorption experiment from the adsorbed amount obtained from the first absorption measurement. The catalysts were pretreated in the identical conditions above mentioned in situ before the measurement.

2.5. EXAFS measurement

X-ray absorption spectra at Rh K-edge and Sn K-edge were measured at the Bl-10B and 14A stations of the Photon Factory in the National Laboratory for High Energy Physics (Proposal No. 92-008 and 94G028) with a positron energy of 2.5 GeV and a storage ring current of 250–350 mA. EXAFS data were collected in a transmission mode using ionization chambers filled with Ar for I_0 signal and Kr for I signal. X-rays from synchrotron radiation were monochromatized by a Si (311) channel cut crystal. The second harmonic is eliminated owing to the extinction rule of the Si (311), and the third and higher harmonics could be neglected owing to the low intensity of the photons with the corresponding energies emitted from the storage ring. The samples were treated in a closed circulating system and/or a Schlenk bottle, and transferred to a glass cell with thin X-ray transparent glass windows for EXAFS meas-

urement without contacting air. EXAFS spectra were taken either at 298 K, 100 K, or 70 K. The resulting data were analyzed by the EXAFS analysis program 'EXAFS2N' in the University of Tokyo. the analysis involves pre-edge extrapolation, background removal by a cubic spline method to extract EXAFS data, and Fourier transformation using a Hanning window function with one-tenth of the Fourier transform range. The typical ranges of Fourier transformation from the k space to the r space are 30–150 nm^{-1} for Rh K-edge EXAFS, and 30–120 nm^{-1} for Sn K-edge EXAFS. The inverse Fourier transformation from the r space to the k space and the curve fitting were carried out to obtain detailed structural information around Rh and Sn atoms.

We used the EXAFS formula based on a single scattering theory by the jth shell atom in the curve fitting analysis of EXAFS data [26],

$$\chi(k_j') = \sum_j N_j F(k_j') \exp(-2k_j'^2\sigma_j^2) \sin(2k_j' R_j + \phi(k_j')) / k_j' R_j^2 \quad (1)$$

$$k_j' = (k_j^2 - 2m\Delta E_{0j}/h^2)^{1/2} \quad (2)$$

where k_j and ΔE_{0j} are the photoelectron wave number and the difference between the origin of the photoelectron wave vector and conventionally determined one, respectively. $F(k_j')$ is the backscattering amplitude function, and $\phi(k_j')$ is the phase shift function. N_j, σ_j, and R_j are the coordination number, the Debye Waller factor and the interatomic distance, respectively. The fitting parameters in the EXAFS analysis are N_j, σ_j, R_j, and ΔE_{0j}. The curve fitting is evaluated by a residual factor (R_f) which is defined as

$$R_f = \int_{k_{min}}^{k_{max}} |k^3\chi^{obs}(k) - k^3\chi^{calc}(k)|^2 dk / \int_{k_{min}}^{k_{max}} |k^3\chi^{obs}(k)|^2 dk \quad (3)$$

Error bars for each parameter can be estimated by stepping each parameter, while optimizing the other parameters, until R_f becomes twice its minimum value. Since no good reference compound was available for Sn–Rh bonding, in the Sn K-edge EXAFS analysis we used the Rh backscattering amplitude derived from Rh foil for Sn–Rh bond because the atomic numbers of Rh and Sn are only different by 5. The phase shifts for this bonding were taken from the tabulated values by Teo and Lee [27]. It is difficult to distinguish Sn–Rh and Sn–Sn bonds from each other by the curve fitting analysis because of the similar values of their fitting parameters. In this article, curve fitting results show the averaged values of Sn–Rh and Sn–Sn bonds. Validity of the theoretically derived parameters was checked by curve fitting analysis of Sn foil [5]. In addition, we performed the curve fitting analysis by FEFF5 for rechecking the analyzed data [28,29]. The R_f of the curve fitting by FEFF was smaller than that by the parameter of Teo and Rh foil, but their fitting results were similar [5].

2.6. Transmission electron microscope (TEM) and analytical TEM

Transmission electron microscope photographs for determination of Rh and Rh–Sn particles sizes were taken by means of JEM-3010 (JEOL) equipment operated at 200 kV. Analytical TEM spectra were also measured with the 7 nm resolution. After the reduction with H_2, the samples were stored under vacuum until the TEM measurements were made. Samples were dispersed in tetrachloromethane by supersonic wave and put on Cu grids for the TEM observation in atmosphere. Sample preparation for TEM was completed within 20 min before putting sample into the TEM chamber, but leading to oxidation of metal particle surfaces. However, the TEM images would be useful for comparing the photographs of bimetallic samples with those of monometallic samples to examine the distribution of particle sizes and to check whether or not the distribution of particle size changes by Sn addition [5]. In addition, the analytical TEM spectra would also be useful for examining whether or not Rh and Sn atoms coexist

in the same particle even with partially oxidized surfaces.

2.7. FT-IR spectra

FT-IR spectra were measured on a Jasco FT-IR 7000 spectrometer in an in situ IR cell which was combined in a closed circulating system. The sample was pressed into a self-supporting disk and put into a slit of the holder in the IR cell. The catalyst was pretreated in situ in the IR cell in the similar conditions above mentioned. IR absorption spectra were taken in a transmission mode and with 2 cm^{-1} resolution.

3. Results and discussion

3.1. Catalytic activities

Fig. 1 shows the dependence of the catalytic activities of the Imp-Rh–Sn/SiO_2 on Sn/Rh atomic ratio. The catalytic activity for styrene hydrogenation decreased monotonously and drastically as the atomic ratio Sn/Rh increased. On the contrary, it was found that the catalytic activity for the hydrogenation of acetophenone increased with an increase of the atomic ratio Sn/Rh, showing a maximum at 0.40 of Sn/Rh. The rate per g-cat for the reaction was larger by a factor of 2 over the Imp-Rh–Sn/SiO_2 (Sn/Rh = 0.4) compared to the Imp-Rh/SiO_2. If the activities are normalized by the number of surface Rh atoms, that is, turnover frequency (TOF), the activity of Imp-Rh–Sn/SiO_2 is 5 times larger than that of Imp-Rh/SiO_2 as discussed hereinafter.

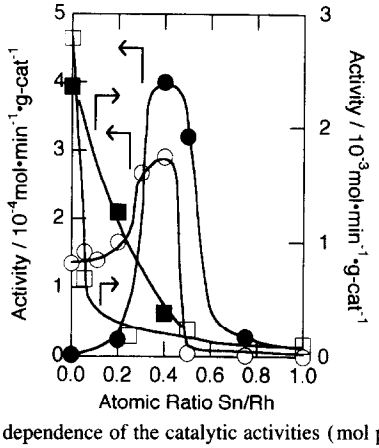

Fig. 1. The dependence of the catalytic activities (mol per min per g-cat) of the Imp-Rh–Sn/SiO_2 catalysts on Sn/Rh atomic ratio at 323 K; ●: 2-butanone (20 ml) hydrogenation with H_2 (1 atm), ○: acetophenone (10 ml) hydrogenation with H_2 (1 atm), ■: 1-hexene (20 ml) hydrogenation with H_2 (1 atm), □: styrene (10 ml) hydrogenation with H_2 (1 atm).

Likewise, the catalytic activity for the hydrogenation of 2-butanone increased as the atomic ratio Sn/Rh increased, also showing a maximum at 0.40 of Sn/Rh. This result was markedly contrasted to the result for the hydrogenation of 1-hexene which shows a monotonous decrease with increasing atomic ratio Sn/Rh increased in Fig. 1. It was observed that the rate per g-cat for 2-butanone hydrogenation was larger by a factor of 200 over the Imp-Rh–Sn/SiO_2 (Sn/Rh = 0.40) compared to the Imp-Rh/SiO_2. This means that the TOF for the Imp-Rh–Sn/SiO_2 catalyst is larger by a factor of 500 than that for the Imp-Rh/SiO_2 catalyst.

As shown in Fig. 1, the Imp-Rh–Sn/SiO_2 showed high activities only in the narrow range of the atomic ratio Sn/Rh for both of acetophenone hydrogenation and 2-butanone hydrogenation. Moreover, the Imp-Rh–Sn/SiO_2 showed the maximum activities at a similar atomic ratio Sn/Rh (= 0.40) for both reactants. These results suggest that particular bimetallic ensembles composed of Rh and Sn atoms are demanded for ketone hydrogenations. It is supposed that these enhancement of the catalytic activities over the active bimetallic ensembles is due primarily to C=O group, because of the maximum activities for both ketone hydrogenations at the similar atomic ratio Sn/Rh (= 0.40) irrespective of aromatic or aliphatic ketones.

3.2. H_2 and CO adsorption

Fig. 2 shows the amounts of H_2 and CO adsorbed on the Imp-Rh–Sn/SiO_2 catalysts as a function of Sn/Rh ratio. The amount of adsorbed H_2 decreased steeply with increasing the Sn/Rh ratio and eventually to nearly zero in the range of Sn/Rh > 0.2. The CO uptake decreased monoto-

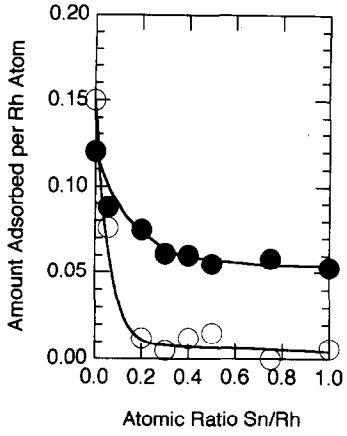

Fig. 2. The amounts of H_2 and CO adsorbed on the Imp-Rh–Sn/SiO_2 catalysts; ●: CO adsorption per total Rh, ○: H_2 adsorption (H atoms) per total Rh.

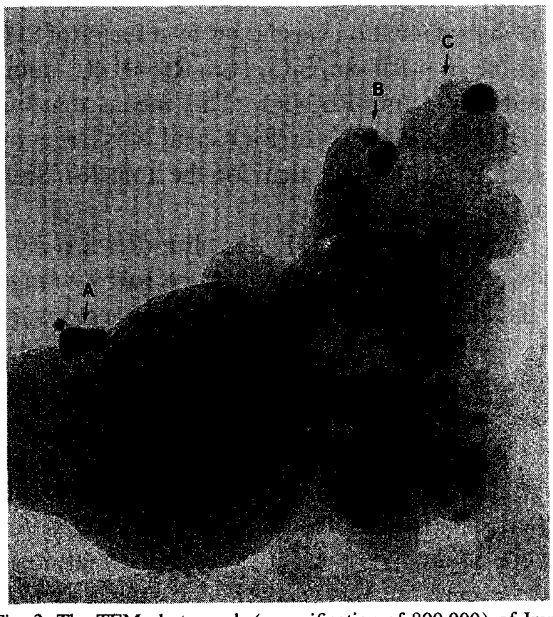

Fig. 3. The TEM photograph (magnification of 800,000) of Imp-Rh–Sn/SiO_2 (Sn/Rh = 0.40).

nously with increasing the Sn/Rh ratio. Since H_2 and CO do not adsorb on Sn, the decrease in the amounts of H_2 and CO adsorbed is due to the decrease in the amount of Rh atoms at the surface of the bimetallic particles on SiO_2. The amounts of CO_2 adsorbed on the Imp-Rh–Sn/SiO_2 catalysts were used in determination of the surface atomic ratio Sn_s/Rh_s as discussed hereinafter.

3.3. TEM and analytical TEM

TEM photographs of the Imp-Rh–Sn/SiO_2 catalysts were taken for determination of particles sizes. Typical TEM image (magnification: × 800,000) for the Imp-Rh–Sn/SiO_2 catalyst with Sn/Rh = 0.40 is shown in Fig. 3. The evaluated average particle sizes (volume–area) of Imp-Rh–Sn/SiO_2 (Sn/Rh = 0, 0.20, 0.40, 1.0) are listed in Table 1. The average particle size of Imp-Rh/SiO_2 estimated by H_2 adsorption was 8 nm, which was similar to 7.5 nm estimated by TEM. We estimated the surface atomic ratio Sn_s/Rh_s of the Imp-Rh–Sn/SiO_2 catalyst (Sn/Rh = 0.40) from the average particle size and the amount of CO adsorption (assuming CO/Rh = 1) according to the formula described by Tomishige et al. [5]. The estimated values are also listed Table 1. The Sn_s/Rh_s ratio in the Imp-Rh–Sn/SiO_2 catalyst (Sn/Rh = 0.40) which showed a maximum catalytic activity is suggested to be about 3/2.

This is based on the assumption that all bimetallic particles have similar composition of Rh and Sn atoms. In order to examine whether the atomic ratio Sn/Rh of each bimetallic particle is the same as whole catalyst, we measured the composition of Rh and Sn elements in selected particles with different particle sizes (e.g., A, B and C in Fig. 3)

Table 1
The averaged particle sizes (volume–area) of the Imp-Rh–Sn/SiO_2 catalysts and their evaluated surface compositions

Catalyst	Averaged diameter [a]/nm	Surface atomic ratio [b] Sn_s/Rh_s
Imp-Rh/SiO_2	7.5	0
Imp-Rh–Sn/SiO_2 (Sn/Rh = 0.2)	9	1.2
Imp-Rh–Sn/SiO_2 (Sn/Rh = 0.4)	11.5	1.5
Imp-Rh–Sn/SiO_2 (Sn/Rh = 1.0)	12	2.4

[a] TEM.
[b] Estimated by the formulas of Tomishige et al. [5].

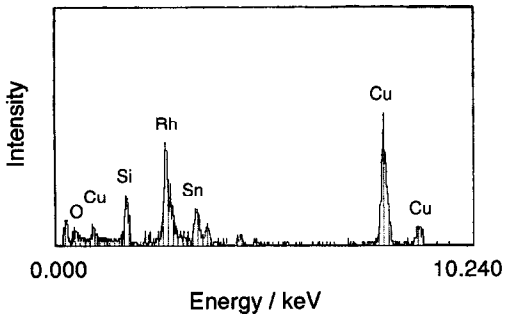

Fig. 4. Analytical TEM spectrum of Imp-Rh–Sn/SiO_2 (Sn/Rh = 0.40) at the arrow C area of Fig. 3 with a 7 nm resolution.

Table 2
Atomic ratio Sn/Rh of each bimetallic particle with different particle sizes in Imp-Rh–Sn/SiO_2 (Sn/Rh = 0, 0.20, 0.40) determined by analytical TEM

Rh–Sn/SiO_2 (Sn/Rh = 0.20)		Rh–Sn/SiO_2 (Sn/Rh = 0.40)		Rh–Sn/SiO_2 (Sn/Rh = 1.0)	
Size/nm	Sn/Rh	Size/nm	Sn/Rh	Size/nm	Sn/Rh
3.1	0.23	3.6	0.41	1.9	0.66
3.5	0.25	4.3	0.45	5.8	0.81
4.4	0.15	7.4	0.47	9.5	0.63
7.3	0.15	10.0	0.40	16.9	0.67
8.5	0.20	10.4	0.40	18.5	0.83

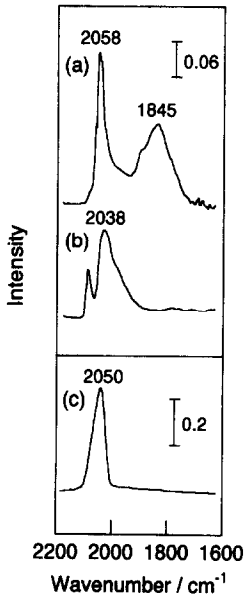

Fig. 5. FT-IR spectra of adsorbed CO on (a) Imp-Rh/SiO_2, (b) Imp-Rh–Sn/SiO_2 (Sn/Rh = 0.40), and (c) CVD-Rh–Sn/SiO_2 (Sn/Rh = 0.45).

by analytical TEM with a 7 nm resolution. Fig. 4 shows an analytical TEM spectrum of the particle (arrow C) of the Imp-Rh–Sn/SiO_2 (Sn/Rh = 0.40). The determined Sn/Rh ratio was 0.41 which is almost the same as the ratio (0.40) of the whole sample. The compositions determined by analytical TEM in three different sample areas for the catalyst with Sn/Rh = 0.40 are shown in Table 2. The Sn/Rh atomic ratio in each bimetallic particle was not very different from each other and similar to 0.40 of the whole catalyst. The results for the catalyst with Sn/Rn = 0.20 are also listed in Table 2. The compositions in these particles are among 0.15–0.25, which are also close to the expected value (0.20). However, the feature for the Sn/Rh = 1.0 catalyst was different from others. The Sn/Rh ratios are observed in the range 0.63–0.83, which are much lower than the expected value 1.0. It is suggested a certain amount of Sn is present out of bimetallic particles in the Imp-Rh–Sn/SiO_2 (Sn/Rh = 1) catalyst.

3.4. FT-IR

Fig. 5 shows FT-IR spectra of CO adsorbed on Imp-Rh/SiO_2 and Imp-Rh–Sn/SiO_2 at 298 K. The assignments which follow are based on the corresponding values reported in the literature [30–36]. On Imp-Rh/SiO_2, linear CO was observed at 2058 cm^{-1} and bridge CO was observed at 1845 cm^{-1}. On the other hand, on Imp-Rh–Sn/SiO_2 linear CO was observed at 2038 cm^{-1} but no bridge CO was observed, suggesting that surface Rh atoms were isolated by the surface Sn atoms. Besides linear CO, a peak at 2092 cm^{-1} and a shoulder at 1985 cm^{-1} were observed with Imp-Rh–Sn/SiO_2 though those intensities were much lower than that of the main linear CO peak. This is contrasted to the case of CVD-Rh–Sn/SiO_2 [5] which shows a single peak in Fig. 5 (c).

3.5. The structure of bimetallic particles in the Imp-Rh–Sn/SiO_2

By analytical TEM spectra Sn atoms were suggested to be approximately uniformly distributed in the bimetallic particles on SiO_2, but there is a question of the location of Sn atoms in the bime-

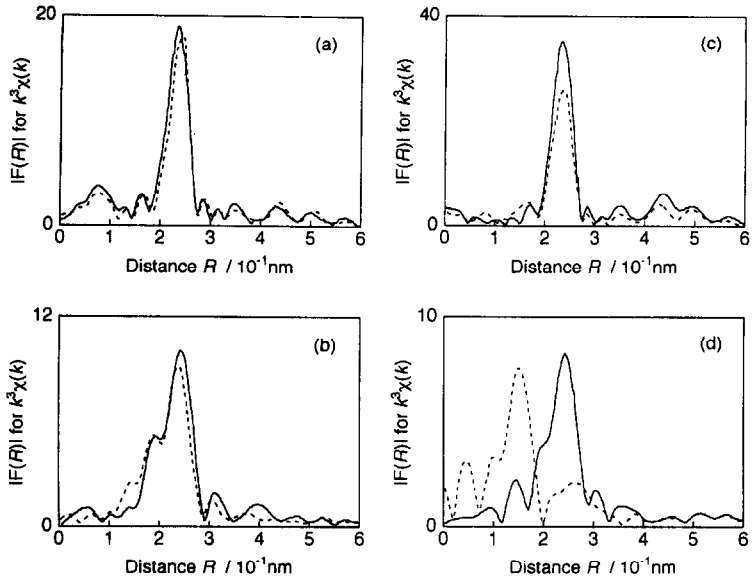

Fig. 6. The Fourier transforms of Sn K-edge and Rh K-edge EXAFS spectra for reduced (solid line) and oxidized (dashed line) Rh–Sn/SiO_2 catalysts. (a) Rh K-edge EXAFS for Imp-Rh–Sn/SiO_2 (Sn/Rh = 0.40) measured at room temperature, (b) Sn K-edge EXAFS for Imp-Rh–Sn/SiO_2 (Sn/Rh = 0.40) measured at room temperature, (c) Rh K-edge EXAFS for CVD-Rh–Sn/SiO_2 (Sn/Rh = 0.30) measured at 70 K, (d) Sn K-edge EXAFS for CVD-Rh–Sn/SiO_2 (Sn/Rh = 0.30) measured at 70 K.

tallic particles, that is, surface and/or bulk. In order to obtain this information we performed the EXAFS analysis. Fig. 6 shows the Fourier transforms of Rh K-edge and Sn K-edge EXAFS spectra of reduced (solid line) and oxidized (dashed line) Rh–Sn/SiO_2 catalysts. The Fourier transform of Rh K-edge EXAFS spectrum of the reduced Imp-Rh–Sn/SiO_2 (Sn/Rh = 0.4) catalyst shows only a peak of Rh–Rh (or –Sn) bond (Fig. 6(a)). The Sn K-edge EXAFS spectrum of reduced Imp-Rh–Sn/SiO_2 (Sn/Rh = 0.4) revealed the existence of only metallic bond Sn–Rh (or –Sn) (Fig. 6(b)). These spectra at both Rh and Sn K-edges demonstrate almost all of the Rh and Sn atoms are situated in the reduced, metallic states. The shapes of the XANES region, particularly the white lines, also suggest that Rh and Sn atoms are metallic.

The reduced catalyst was exposed to air at room temperature. The intensities of the EXAFS Fourier transforms at Rh and Sn K-edged for the oxidized catalyst a little decreased compared to those for the reduced catalyst (Fig. 6(a) and (b)). In addition, a new peak appeared in the EXAFS Sn K-edge Fourier transform (Fig. 6(b)). The new peak was analyzed by the curve-fitting technique and assigned to be Sn–O bond at 0.208 nm with the coordination number of 1.2 These changes in Fig. 6(a) and (b) were small and further examined by using the CVD-Rh–Sn/SiO_2 catalyst. Upon exposure of the reduced CVD-Rh–Sn/SiO_2 catalyst to air at room temperature, the Sn–Rh (or –Sn) bonds completely disappeared and instead the Sn–O bonds at 0.205 nm (coordination number: 4.1) appeared, which reveals that all of the Sn atoms were located at the surface of bimetallic particles [5,10]. The Sn–O bond distance 0.205 nm is almost the same as 0.208 nm for Imp-Rh–Sn/SiO_2. Accordingly, most of Sn atoms in Imp-Rh–Sn/SiO_2 are concluded to be located inside the bimetallic particles and a part of the Sn atoms are present at the outmost layer of the particles, because only the atoms at the outmost layer of the bimetallic particles are oxidized when exposed to air at room temperature [5,8–10].

3.6. Acetophenone hydrogenation on CVD-Rh–Sn/SiO_2

We used the Imp-Rh–Sn/SiO_2 catalysts as mentioned above. But the Imp-Rh–Sn/SiO_2 cat-

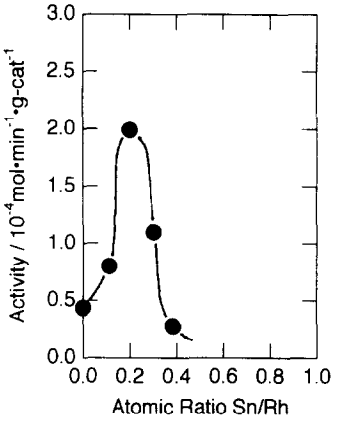

Fig. 7. Catalytic activities (product mol per min per g-cat) of the CVD-Rh–Sn/SiO_2 catalysts for acetophenone hydrogenation at 323 K as a function of Sn/Rh atomic ratio; H_2 = 1 atm, acetophenone = 20 ml.

alysts are not useful in investigation of the surface, particularly in the EXAFS study, because Sn atoms are located both at the surface and in the bulk of the bimetallic particles. So, we have used the CVD-Rh–Sn/SiO_2 catalysts as model to explore the enhancing mechanism by Sn additive. The CVD-Rh–Sn/SiO_2 catalysts have been well characterized [5,6,9,10].

Fig. 7 shows catalytic activities of the CVD-Rh–Sn/SiO_2 catalysts prepared by using the reaction of $Sn(CH_3)_4$ vapor with Rh particles on SiO_2, as a function of Sn/Rh ratio. The catalytic activity for acetophenone hydrogenation increased as the atomic ratio Sn/Rh increased, showing a maximum activity at ca. 0.2 of Sn/Rh. The ratio 0.2 corresponds to 1:1 of Sn_s:Rh_s at the surface as estimated from the article by Tomishige et al [5]. This value is a little different from 1.5:1 (3:2) for Imp-Rh–Sn/SiO_2 (Sn/Rh = 0.40), which showed a maximum activity for acetophenone hydrogenation as already mentioned. Considering uncertainty of the maximum point in Fig. 7 and of the surface composition from TEM and adsorption measurement, it is valid that active bimetallic ensembles on SiO_2 have the composition of Sn_s/Rh_s = 1–1.5.

3.7. Observation of Sn–acetophenone interaction by EXAFS

We measured a Sn K-edge EXAFS spectrum on CVD-Rh–Sn/SiO_2 (Sn/Rh = 0.2) after acetophenone adsorption in order to investigate the interaction of Sn with acetophenone. Fig. 8 shows the Fourier transforms of the Sn K-edge EXAFS spectrum on CVD-Rh–Sn/SiO_2 (Sn/Rh = 0.2) after and before acetophenone adsorption. There are three peaks at 0.14, 0.19 and 0.24 nm (phase shift: uncorrected) in Fig. 8. The third peak is essentially the same as that for the reduced CVD-Rh–Sn/SiO_2 catalyst, which has been characterized by two kinds of Sn–Rh (or –Sn) (shorter and longer) bonds [5], where the first bimetallic layer is relaxed far from the bulk Rh fcc structure. Thus, similarly, the shorter bond at 0.270 nm is assigned to Sn–Rh (or –Sn) in the first bimetallic layer and the longer bond at 0.286 nm is attributed to Sn–Rh (2nd layer) due to the relaxed bimetallic structure of the first layer (Table 3). The EXAFS data reveal that the surface structure retains after acetophenone adsorption. The first peak and second peak may be tentatively assigned to Sn–O or Sn–C bonds due to interaction of Sn atom with the carbonyl group of acetophenone. In fact, no Sn–O or Sn–C bond in this region was observed with styrene adsorption as shown in Table 3. We also measured a Sn K-edge EXAFS spectrum on CVD-Rh–Sn/SiO_2 (Sn/Rh = 0.2) after 2-butanone adsorption. But no Sn–O or Sn–C bond was observed as shown in Fig. 9, which is similar to the Fourier transform for the catalyst before adsorption (Table 3). The adsorption packing at the bimetallic surface may be more fixed with acetophenone than with 2-butanone, resulting in observation of the direct interaction of Sn atoms with acetophenone. The first and second peaks

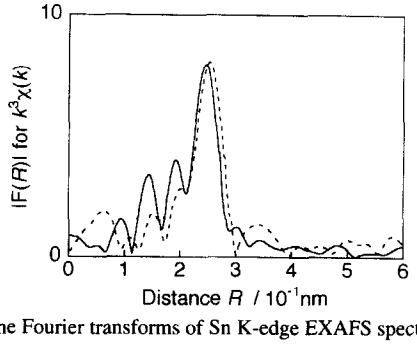

Fig. 8. The Fourier transforms of Sn K-edge EXAFS spectra at 100 K for CVD-Rh–Sn/SiO_2 (Sn/Rh = 0.20) before (dashed line) and after (solid line) acetophenone adsorption.

Table 3
Curve fitting results of the Sn K-edge EXAFS data measured at 100 K for the CVD-Rh–Sn/SiO_2 catalysts (Sn/Rh = 0.20)

Sample	Bond assignment	C.N. [a]	Bond distance R/nm	ΔE_0 [b]/eV	σ [c]/nm	R_f [d]/%
(A)	Sn–Rh (or –Sn)	5.2	0.270	2.8	0.0102	4.0
	Sn–Rh (or –Sn)	2.0	0.286	9.5	0.0110	
(B)	Sn–Rh (or –Sn)	5.9	0.270	4.5	0.0102	1.6
	Sn–Rh (or –Sn)	2.8	0.286	1.5	0.0110	
	Sn–O	0.6	0.198	−4.8	0.0060	
	Sn–C	0.8	0.262	−4.2	0.0060	
(C)	Sn–Rh (or –Sn)	5.0	0.270	3.8	0.0102	7.4
	Sn–Rh (or –Sn)	2.0	0.287	8.7	0.0110	
(D)	Sn–Rh (or –Sn)	5.7	0.271	4.7	0.0102	4.4
	Sn–Rh (or –Sn)	3.0	0.286	4.7	0.0110	

(A): after reduction, (B): after acetophenone adsorption, (C): after styrene adsorption, (D): after 2-butanone adsorption.
Fourier transform range: 30–120 nm^{-1}, Fourier filtering range: 0.10–0.32 nm.
[a] Coordination number.
[b] The difference between origins of photoelectron wave vector.
[c] Debye Waller factor.
[d] R factor.

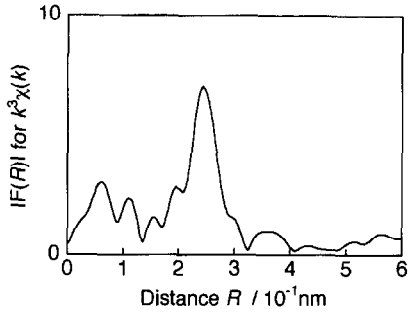

Fig. 9. The Fourier transform of Sn K-edge EXAFS spectra measured at 100 K for CVD-Rh–Sn/SiO_2 (Sn/Rh = 0.20) after 2-butanone adsorption.

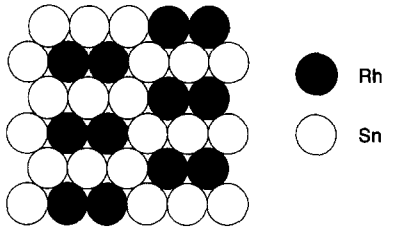

Fig. 10. A bimetallic ensemble model with $Sn_s/Rh_s = 1.5$.

may be ascribed to the carbonyl group of acetophenone because those peaks were not observed in the case of styrene. We performed the curve fitting analysis over the whole range assuming Sn–O, Sn–C, Sn–Rh (–Sn), and Sn–Rh (–Sn). As the maximum number of independent parameters (N_I) is calculated to be 14.6 in our case ($\Delta k = 90$ nm^{-1}, $\Delta R = 0.22$ nm) [37], it is not valid to fit the four bonds from the present EXAFS data. In the present EXAFS analysis, the Debye Waller factors were fixed as shown in Table 3, while other parameters were optimized. Furthermore, we performed the curve fitting, moving freely C.N., R, ΔE_0, and σ, while the values for Sn–Rh (–Sn) and Sn–Rh (–Sn) were fixed at the values determined for the reduced CVD-Rh–Sn/SiO_2. The results were very close to each other. Therefore, we propose the existence of direct interaction between Sn atom and the carbonyl group. However, the EXAFS analysis can not discriminate O and C atoms.

3.8. Promotion mechanism

The optimum surface composition for ketone hydrogenations was estimated to be Sn_s/Rh_s = ca. 1.5. A bimetallic ensemble model with $Sn_s/Rh_s = 1.5$ is illustrated in Fig. 10, where Sn atoms and Rh atoms were well mixed each other, because Sn–Rh bond is more stable than Sn–Sn bond or Rh–Rh bond. This assumption is supported by FT-IR spectra of adsorbed CO, which showed no large Rh ensemble sites. Moreover, it has been reported that various transition metals form stable surface alloys with Sn, showing the ordered $\sqrt{3} \times \sqrt{3}$ surface alloy structures of Sn/Cu (111), Sn/Ni (111), and Sn/Pt (111) [38]. In the case of the

Sn/Pd system, *c* (2×2)–Sn/Pd (100) surface alloy with the $Sn_s/Rh_s = 1$ is observed [39]. In the Sn/Ru system, ($\sqrt{3}\times\sqrt{3}$)–Sn/Ru (001) is observed at $Sn_s/Ru_s = 2.0$ [40]. Although the surface alloy structure of Sn/Rh (111) has not been reported as far as we know, analogous surface alloy structures are likely to be formed. Tomishige et al. proposed the bimetallic ensemble model ($Sn_s/Rh_s = 3$) in order to explain the high activity of CVD-Rh–Sn/SiO_2 for NO–H_2 reaction [5,9], where direct bonding of Sn and O of bent NO at 0.256 nm was observed by in situ EXAFS [6]. But the catalyst with $Sn_s/Rh_s = 3$ shows little activity for ketone hydrogenations. The catalyst with $Sn_s/Rh_s = 2$ also shows little activity for ketone hydrogenations. At these surfaces most of Rh atoms are completely isolated. These results suggest that the Rh–Sn ensembles in which Rh atoms are completely isolated are inactive for ketone hydrogenations. The catalysts with surface atomic ratio $Sn_s/Rh_s < 0.5$ also shows less activity, which suggests that isolated Sn atoms do not promote ketone hydrogenations efficiently.

Next, we consider adsorption structure of acetophenone. The bond lengths determined from EXAFS are listed in Table 3. The bond length of 0.262 nm for Sn–O or Sn–C is rather large compared with 0.205 nm in SnO_2 or 0.222 nm in SnO, while the bond length of 0.198 nm is similar to Sn–O in SnO_2. Thus four structures are possible; di-σ bond structure (carbonyl carbon–Rh and carbonyl oxygen–Sn bonds), di-σ bond structure (reverse to the above bonding), coordination bonding of carbonyl oxygen to Rh, and coordination bonding of carbonyl oxygen to Sn. It was reported that the coordinated bond length of Sn–O in dichloro(1,4-dioxane)tin(II) is 0.2527 nm. The 0.262-nm bond is much longer than the coordination-type bonding and the shorter bond at 0.198 nm cannot be explained by this bonding type. It is unlikely that fragment from acetophenone makes the 0.198-nm bond with Sn atom on Rh–Sn/SiO_2 because Sn atoms have much less activity for such hydrogenolysis than Rh atoms. Furthermore, the observation of definite Sn–O or Sn–C bonds by EXAFS is most likely to be due to more rigid structure. Thus the formation of di-σ bond is suggested upon acetophenone adsorption on Rh–Sn/SiO_2. In order to examine which di-σ structure is dominant, we attempted a FT-IR study of adsorbed ketone. But intense absorption of ketone adsorbed on the carrier prevented adsorption of ketone on metal particles from being observed.

Although Sn–O bond and Sn–C bond are indistinguishable in EXAFS analysis, the structure shown in Fig. 11 is likely because Sn has more affinity with O than Rh [5]. Bond dissociation energy of Sn–C in $Sn(CH_3)_4$ is 272 kJ mol^{-1} while bond dissociation energy of Sn–O in $(CH_3)_3SnOC_2H_5$ is 351 kJ mol^{-1} [41]. On the other hand, bond dissociation energy of Rh–C in (OEP)Rh–$CH(CH_2)_3CH_3$)OH (OEP: octaethylporphyrin) is 190 kJ mol^{-1} and bond dissociation energy of Rh–O in (OEP)Rh–OCH_2R is 210–230 kJ mol^{-1} [42]. The Rh^+–C bond dissociation energy in Rh^+–CH_3 was also estimated to be 196 ± 21 kJ mol^{-1} by ion beam study [43]. These data indicate that the formation of Sn–O and Rh–C bonds is favored over that of Sn–C and Rh–O bonds by about 25–90 kJ mol^{-1}. Moreover, it is known that Sn–H reacts with ketones to form Sn–alkoxide complexes [44] and that (OEP)Rh–H reacts with aldehydes to form Rh–hydroxyalkyl complexes [45]. Thus the structure shown in Fig. 11 is likely to be a favorable reaction intermediate for ketone hydrogenation.

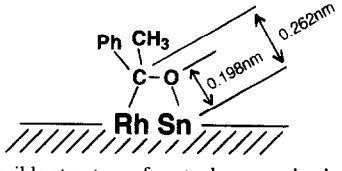

Fig. 11. A possible structure of acetophenone adsorbed on Rh–Sn/SiO_2.

4. Conclusions

1. Sn added to Rh/SiO_2 promotes the hydrogenation reaction of 2-butanone and acetophenone. Considerable enhancement of the rate (TOF) was observed; 500 times for 2-butanone hydrogenation and 5 times for acetophenone hydrogenation on Imp-Rh–Sn/SiO_2 ($Sn/Rh = 0.4$).
2. The dependence of the catalytic activity on the Sn content showed the presence of an optimum Sn quantity for ketone hydrogenations.
3. EXAFS revealed that Sn and Rh are situated in the metallic states.
4. H_2 and CO adsorption and FT-IR spectra suggested that surface Rh atoms in Imp-Rh–Sn/SiO_2 were isolated by the surface Sn atoms.
5. The optimum surface atomic ratio Sn_s/Rh_s for ketone hydrogenations was estimated to be 3/2.
6. The active bimetallic ensemble for ketone hydrogenations was supposed to be Rh dimers surrounded by eight Sn atoms.
7. Oxygen of C=O group of adsorbed acetophenone was suggested to make a bond with Sn atom by in situ Sn K-edge EXAFS of the well characterized CVD-Rh–Sn/SiO_2 catalyst prepared by using $Sn(CH_3)_4$ vapor.

References

[1] W.M.H. Sachtler and R.A. van Santen, Adv. Catal., 26 (1977) 69.
[2] B. Imelik, C. Naccache, G. Coudurier, H. Praliaud, P. Meriaudeau, P. Gallezot, G.A. Martin and J.C. Vedrine (Eds.), Metal–Support and Metal–Additive Effect in Catalysis, Studies in Surface Science and Catalysis, Vol. 11, Elsevier, Amsterdam, 1982.
[3] M. Masai, K. Mori, H. Muranoto, T. Fujikawa and S. Ohnaka, J. Catal., 38 (1975) 128.
[4] M. Masai, K. Honda, A. Kubota, S. Ohnaka, Y. Nishikawa, K. Nakahara, K. Kishi and S. Ikeda, J. Catal., 50 (1977) 419.
[5] K. Tomishige, K. Asakura and Y. Iwasawa, J. Catal., 149 (1994) 70.
[6] K. Tomishige, K. Asakura and Y. Iwasawa, J. Catal., to be submitted.
[7] K. Tomishige, K. Asakura and Y. Iwasawa, Chem. Lett., (1994) 235.
[8] K. Tomishige, K. Asakura and Y. Iwasawa, J. Chem. Soc., Chem. Commun., (1993) 184.
[9] K. Tomishige, K. Asakura and Y. Iwasawa, Catal. Lett., 20 (1993) 15.
[10] K. Tomishige, K. Asakura and Y. Iwasawa, Shokubai, 35 (1993) 398.
[11] J.P. Candy, A.E. Mansour, O.A. Ferretti, G. Mabilon, J.P. Bournonville, J.M. Basset and G. Martino, J. Catal., 112 (1988) 201.
[12] J.P. Candy, O.A. Ferretti, G. Mabilon, J.P. Bournonville, A.E. Mansour, J.M. Basset and G. Martino, J. Catal., 112 (1988) 210.
[13] M. Agnelli, J.P. Candy, J.M. Basset, J.P. Bournonville and O.A. Ferretti, J. Catal., 121 (1990) 236.
[14] J.M. Basset, J.P. Candy, P. Louessard, O.A. Ferretti and J.P. Bournonville, Wissenschaftliche Zeitschrift, TH Leuna-Merseburg, 32 (1990) 657.
[15] S. Galvagno, Z. Poltarzewski, A. Donato, G. Neri and R. Pietropaolo, J. Chem. Soc., Chem. Commun., (1986) 1729.
[16] Z. Poltarzewski, S. Galvagno, R. Pietropaolo and P. Staiti, J. Catal., 102 (1986) 190.
[17] S. Galvagno, A. Donato, G. Neri, R. Pietropaolo and G. Capannelli, J. Mol. Catal., 78 (1993) 227.
[18] T.B.L.W. Marinelli, J.H. Vleeming and V. Ponec, in L. Guczi, F. Solymosi and P. Tétényi (Eds.), Reaction of Multifunctional Organic Compounds – Hydrogenation of Acrolein on Modified Pt-Catalysts, in Proceedings of the 10th International Congress on Catalysis, Studies in Surface Science and Catalysis, Vol. 75B, Elsevier, Amsterdam, 1993, p. 1211.
[19] T.B.L.W. Marinelli, V. Ponec, G.G. Raab and J.A. Lercher, Furfural–Hydrogen Reactions, Manipulation of Activity and Selectivity of the Catalyst, in M. Guisnet, J. Barbier, J. Barrault, C. Bouchoule, D. Duprez, G. Pérot and C. Montassier (Eds.), Proceedings of the 3rd International Symposium of Heterogeneous Catalysis and Fine Chemicals, Studies in Surface Science and Catalysis, Vol. 78, Elsevier, Amsterdam, 1993, p. 195.
[20] T.B.L.W. Marinelli, S. Nabuurs and V. Ponec, (to be published).
[21] G.G. Raab, M. Englisch, T.B.L.W. Marinelli and J.A. Lercher, Selective Hydrogenation of Crotonaldehyde over Pt derived Catalysts, in M. Guisnet, J. Barbier, J. Barrault, C. Bouchoule, D. Duprez, G. Pérot and C. Montassier (Eds.), Proceedings of the 3rd International Symposium of Heterogeneous Catalysis and Fine Chemicals, Studies in Surface Science and Catalysis, Vol. 78, Elsevier, Amsterdam, 1993, p. 211.
[22] B. Didillon, A.E. Mansour, J.P. Candy, J.-M. Basset, F.L. Peltier and J.P. Bournonville, New Organometallic Active Sites Obtained by Controlled Surface Reaction of Organonmetallic Complexes with Supported Metal Particles, in Preparation of Catalysts V, Studies in Surface Science and Catalysis, Vol. 63, Elsevier, Amsterdam, 1991, p. 717.
[23] B. Didillon, J.P. Candy, A.E. Mansour, C. Houtmann and J.-M. Basset, J. Mol. Catal., 74 (1992) 43.
[24] B. Didillon, C. Houtmann, T. Shay, J.P. Candy and J.-M. Basset, J. Am. Chem. Soc., 115 (1993) 9380.
[25] J.P. Candy, B. Didillon, E.L. Smith, T.B. Shay and J.-M. Basset, J. Mol. Catal., 86 (1994) 179.
[26] B.K. Teo, EXAFS: Basic Principles and Data Analysis, Springer-Verlag, New York, 1985, p. 26.
[27] B.K. Teo and P.A. Lee, J. Am. Chem. Soc., 101 (1979) 2815.

[28] J.J. Rehr, J.M. Leon, S.I. Zabinsky and R.C. Albers, J. Am. Chem. Soc., 113 (1991) 5135.
[29] J.M. Leon, J.J. Rehr, S.I. Zabinsky and R.C. Albers, Phys. Rev., B44 (1991) 4146.
[30] A.Y. Yang and C.W. Garland, J. Phys. Chem., 61 (1957) 1505.
[31] J.T. Yates, Jr., T.M. Duncan, S.D. Worley and R.W. Vaughan, J. Chem. Phys., 70 (1979) 1219.
[32] R.R. Cavanagh and J.T. Yates, Jr., J. Chem. Phys., 74 (1981) 4150.
[33] F. Solymosi and M. Pasztor, J. Am. Chem. Soc., 89 (1985) 4789.
[34] H.F.J. van't Bilk, J.B.A.D. van Zon, J.C. Vis, D.C. Koningsberger and R. Prins, J. Am. Chem. Soc., 107 (1985) 3139.
[35] P. Basu, D. Panayotov and J.T. Yates, Jr., J. Am. Chem. Soc., 110 (1988) 2074.
[36] J.A. Anderson and F. Solymosi, J. Chem. Soc., Faraday Trans., 87 (1991) 3435.
[37] E.A. Stern, Phys, Rev., B 48 (1993) 9825.
[38] S.H. Overbury and Y. Ku, Phys. Rev., B 46 (1992) 7868.
[39] A.D. Logan and M.T. Paffett, J. Catal., 133 (1992) 179.
[40] M.T. Paffett, A.D. Logan and T.N. Taylor, J. Phys. Chem., 97 (1993) 690.
[41] R.A. Jackson, J. Organomet. Chem., 166 (1979) 17.
[42] B.B. Wayland, Polyhedron, 7 (1988) 1545.
[43] M.L. Mandich, L.F. Halle and J.L. Beauchamp, J. Am. Chem. Soc., 106 (1984) 4403.
[44] A.G. Davies and P.J. Smith, in Comprehensive Organometallic Chemistry, Vol. 2, Pergamon Press, Oxford, 1982, p. 519.
[45] B.B. Wayland, B.A. Woods and V.M. Minda, J. Chem. Soc., Chem. Commun., (1982) 634.